Colloid Polym Sci (2011) 289:1347–1359
DOI 10.1007/s00396-011-2451-7

ORIGINAL CONTRIBUTION

# Effect of melt viscosity on the crystallization kinetics of pre-sheared metallocene polyethylene melts

**Joanna Krakowiak · José A. Martins · Weidong Zhang**

Received: 4 March 2011 / Revised: 11 May 2011 / Accepted: 20 May 2011 / Published online: 14 June 2011


**Abstract** This work aims to verify the impossibility mentioned in the literature of saturating the crystallization kinetics of pre-sheared metallocene polyethylene melts. Similarly to results reported for other materials, and contrary to other published works, an acceleration of crystallization kinetics with the increase of shear strain and its saturation at large strain values was found. Similar strain values, with the same temperature variation, were evaluated with independent experiments using different devices, which allowed us to identify the steady state as the melt state responsible for the saturation of crystallization kinetics. Since this is a partially disentangled melt state, with viscosity lower than that of fully entangled (relaxed) melts, we assign the acceleration of crystallization kinetics by application of shear, and its saturation, mainly to the facilitated diffusion of chain segments to the lamellae growth front. This conclusion is supported additionally with the experimental results of other authors.

**Keywords** Melt memory · Crystallization · Saturation · Metallocene

**Electronic supplementary material** The online version of this article (doi:10.1007/s00396-011-2451-7) contains supplementary material, which is available to authorized users.

J. Krakowiak · J. A. Martins · W. Zhang
Departamento de Engenharia de Polímeros,
Universidade do Minho,
Campus de Azurém,
4800-058 Guimarães, Portugal

J. Krakowiak · J. A. Martins (✉) · W. Zhang
CICECO, Universidade de Aveiro,
3810-193 Aveiro, Portugal
e-mail: jamartins@dep.uminho.pt

## Introduction

The heterogeneous Ziegler–Natta catalyst was developed in the early 1950s. A material synthesized with these catalysts has a polydispersity index higher than 3 and the co-monomer is incorporated heterogeneously along the chain. The homogeneous metallocene type catalyst was developed in the 1980s [1]. Because metallocene catalysts are single-site catalysts, they allow linear polymers with lower polydispersity index (around 2) and well-defined architecture to be obtained.

Most studies with these polymers have been focused on the long- or short-chain branching effect on the rheological properties and solid-state morphology. Wang et al. [2] studied the effect of highly short-chain branching on the solid-state morphology development of metallocene-based polyethylene with narrow molecular weight distribution and an ethyl branching content of 10.4 mol%, which yields a uniform distribution of short-chain branches along the chain. Upon crystallization, a network structure was found at the solid state where small crystals acted as "physical crosslinks" and ethylene sequences provided the connections. Based on the DSC stepwise fractionation method, the length of crystallisable ethylene sequences was found to be too short for developing a fold similar to that observed in lamellar crystals. Wang et al. named those structures fringed-micelle-like crystals and determined their thickness by small-angle X-ray scattering to be around 26 Å.

The rheological behaviour at the molten state and in the vicinity of liquid-to-solid transition (gel point) was studied by Gelfer et al. [3]. They investigated the viscoelastic properties of ethylene–hexene copolymers of linear low-density polyethylene (LLDPE) synthesized with metallocene and Ziegler–Natta catalysts, differing in branching degree, and of their blends with linear polymer chains of

high density polyethylene (HDPE). The ZN-LLDPE with a bimodal intermolecular branching distribution has relatively high fractions of both low-branched chains (branching content $x<1$ mol%) and highly branched chains ($5<x<12$ mol%). The branching distribution of M-LLDPE used was unimodal, with an average branching of 2.61 mol%. For reference materials, they used un-branched polyethylenes, ZN-HDPE and M-HDPE. It was found that the rheological behaviour in the vicinity of liquid–solid transition was determined by the content of linear molecules rather than by the overall branching. This conclusion was reached from experiments with blends having different contents of the two polymers, one un-branched (ZN-HDPE) and the other branched (M-LLDPE). For ZN-HDPE/M-LLDPE blends, the increase of ZN-HDPE content (or content of linear molecules) originated the narrowing of solidification interval when compared with the solidification interval width of M-LLDPE or ZN-LLDPE. It was also found that polymers synthesized with Ziegler–Natta catalysts have lower flow activation energy than metallocene-based polymers and that the onset of shear thinning occurs earlier for Ziegler–Natta polyethylene (ZNPE). No explanation was provided for the different flow activation energy, although the lower flow activation energy of ZN-LLDPE could be understood by the higher branching content of this polymer.

The effect of catalyst type on the melt morphology development was studied by Rastogi et al. [4, 5]. They used two different ultra-high molecular weight polyethylenes (UHMW-PE), one obtained from highly active heterogeneous Ziegler–Natta catalysts at high polymerization temperatures and the other from single-site catalysts at low polymerization temperatures. Because of the high catalytic activity and high polymerization temperature, the ZNPE crystalline lamellae and the amorphous regions are composed of different chains. On the contrary, the whole crystal of metallocene samples consists of a single chain.

Different melt states were obtained for these two PEs. For ZNPE, regardless of the heating mode used, slow heating rate or fast heating rate, a homogeneous melt was always obtained. By homogeneous, it is meant that the melt has a regular distribution of entanglements along the chain. On the other hand, fast melting of metallocene polyethylene (MPE) yields also a homogeneous melt, but melting with slow heating rate yields a heterogeneous melt. In this last case, the homogeneous melt state is reached only after a long heating time. Metallocene polyethylene melts have lower viscosity than the melts of Ziegler–Natta polyethylenes, which was assigned to the disentangled chains of metallocene polyethylene. In agreement with a previous work [6], it was also found that the disentangled chains of MPE crystallize faster than the entangled chains of ZNPE. However, the physical reason for the faster crystallization kinetics in disentangled melts was not explicitly assigned to their lower viscosity. We discuss this result further.

A description of pre-shear history influence on the crystallization of two hexane copolymers, a Ziegler–Natta-catalyzed linear low-density polyethylene (LLDPE) and a linear metallocene of similar melt flow index, density and molecular weight (~$10^5$ g/mol), but of different molecular weight distributions (3.4 and 2.1, respectively), was made by Chai et al. [7]. They used a Linkam shearing cell with quartz windows in close thermal contact with the silver block heaters. The polymer sample was sheared at the test temperature ($T_s$=190, 170 and 150 °C) with a given shear rate (from 1 to 18 $s^{-1}$) during a shearing time, $t_s$, left there for a waiting time in the range of 0–10 min and cooled down to 90 °C at a controlled cooling rate of 20 °C/min. Small-angle light scattering patterns were recorded during the whole process.

The spherulite radius of ZNPE was found to decrease with pre-shear and saturate at a strain of ~$10^3$ s.u. with a value of half the spherulite radius without shear ($R_0\approx$ 12 μm). No spherulite radius variation with pre-shear was observed for the linear metallocene PE ($R_0\approx$3 μm). It was also found that the waiting (or annealing) time at the melt temperature after shear affects the spherulite size of ZNPE. The decrease of spherulite radius is more pronounced for a short waiting time, below a limiting value, while for a longer waiting time no change was observed. According to Chai et al., this limiting waiting time value represents the largest relaxation time of ZNPE, which, however, is 20 times the longest relaxation time evaluated by small-amplitude oscillatory shear experiments.

In our view, the three important results of Chai's work are: (1) the conclusion that the establishment of steady state in ZNPE requires a large amount of shear deformation, around $10^3$ s.u.; (2) the observation that after the attainment of this state no changes in crystallization occur, that is, further shear does not change the size of spherulites; and (3) the observation that annealing the pre-sheared melts for a long time erases flow deformation effects on the final spherulite size. To the best of our knowledge, the physical reason for this behaviour was not explained so far.

The different results obtained by Chai et al. for Ziegler–Natta and metallocene-based polyethylenes were one important motivation for the experiments described below. It is known that linear polymer chains, regardless of the catalyst type used for their synthesis, can reach in shear flows a well-defined steady state. Because it was demonstrated in previous works that steady state is the melt state responsible for the saturation of crystallization of polymers sheared above their equilibrium melting temperature [6, 8], it was surprising to find the conclusion that the crystallization kinetics of pre-sheared metallocene-based polyethyl-

ene cannot saturate. The experimental results presented below aim to demonstrate the invalidity of this conclusion and prove that metallocene-based PE behaves similarly to any other linear polymer chains.

We present, in addition, a physical explanation for the acceleration of crystallization kinetics from pre-sheared melts and its slowing down by annealing of the melt. A preliminary attempt to explain these results was presented in a previous work [9]. We complement here that explanation with additional results of our own and results of other authors obtained in similar experimental conditions. It must be stressed also that, although we analyse the effect of pre-shearing the melt on the crystallization kinetics, we do not fit our work within the area of shear-induced crystallization. The recording of crystallization kinetics in our experiments was done in the absence of flow. We study, with detail, the ability of melt, sheared above its melting temperature, to store the memory of previous deformations and the effect of this deformation on the crystallization kinetics. The effect of short-term shearing at the crystallization temperature and melt deformations applied below the melting temperature was studied by other workers [10–13].

## Experimental

### Materials characterization

Two different polyethylenes were used in this work, a Ziegler–Natta polyethylene and a metallocene polyethylene. Some material's properties are presented in Table 1. Both polymers have a similar density measured at 25 °C. ZNPE has an average molecular weight ($M_w$) of ~114,650 g/mol and a molecular weight distribution ($M_w/M_n$) of 3.7; MPE has $M_w \approx 106{,}100$ g/mol and $M_w/M_n \sim 2.3$. The equilibrium melting temperature, evaluated following the Hoffman–Weeks extrapolation procedure, is also in Table 1. It is higher for ZNPE. Oxidation induction time evaluated by DSC ($T$=200 °C, gas—nitrogen and oxygen, flow rate of 50 ml/min, heating rate 10 °C/min) is equal to 2.13 min for ZNPE and 30.19 min for MPE.

$^{13}$C NMR experiments performed in the Polish Academy of Sciences (Lodz, Poland) allowed to conclude that ZNPE is a copolymer of ethylene and octene, with 3.03 mol% of octene and has 88.84 wt% of carbon atoms in ethylene sequences and 11.16 wt% of carbon atoms in octene, while MPE is a copolymer of ethylene and hexene with 2.6 mol% of hexene and has 92.6 wt% of carbon atoms in ethylene sequences and 7.4 wt% of carbon atoms in hexene.

### Thermal analysis experiments after shear

The flow effects on crystallization kinetics were evaluated under quiescent conditions in the capillary channel of a shear DTA instrument by measuring the difference of temperature between the sample in the capillary and a reference following the same temperature program [14]. Deformations were applied by a piston to the molten polymer stored in an accumulator that flows, by a conical channel, to a capillary where thermal analysis measurements were performed. All of these measurements were performed in the absence of flow. Therefore, only the flow effects were recorded.

The melt memory protocol followed is illustrated in Fig. 1. At the start of the experiment, all the different parts are heated up to a selected temperature, above the polymer melting temperature. Controlled deformations, with different shear rates and shearing times, are applied to the polymer melt stored in the accumulator. After the desired shearing, the valves at the entrance and exit of the capillary are closed for stopping the flow and promoting the thermal insulation between the accumulator and capillary. This channel is then cooled to the crystallization temperature and the effect of flow deformations on the crystallization kinetics is recorded by a set of thermocouples along the length of the capillary. Similarly to the procedure used in commercial DTAs and DSCs, the evaluation of crystallization kinetics was done by the integration of the exothermal peaks recorded.

Since during the shear deformation the melt is continually pumped from the accumulator to the capillary and all different sections are maintained at the same temperature, the overall melt deformation is evaluated by adding the deformations at the different sections. A detailed description of the evaluation of the strain in each section is provided in the supplementary information to this work. This protocol allows us to impose a well-defined history at different melt temperatures and analyse the effect of different deformations on the crystallization development.

**Table 1** Density, average molecular weights, polydispersity, equilibrium melting temperature and oxidation induction time for ZNPE and MPE. The density, $\rho$, was measured at 25 °C

| Polymer | $\rho$ (g/cm$^3$) | $M_n$ (g/mol) | $M_w$ (g/mol) | $M_z$ (g/mol) | $M_w/M_n$ | $T_m$ (ºC) | $t_{In}$ (min) |
|---|---|---|---|---|---|---|---|
| ZNPE | 0.8389±0.003752 | 30,700 | 114,650 | 438,200 | 3.7 | 127.7 | 2.13 |
| MPE | 0.8358±0.001952 | 46,100 | 106,100 | 185,000 | 2.3 | 125.5 | 30.19 |

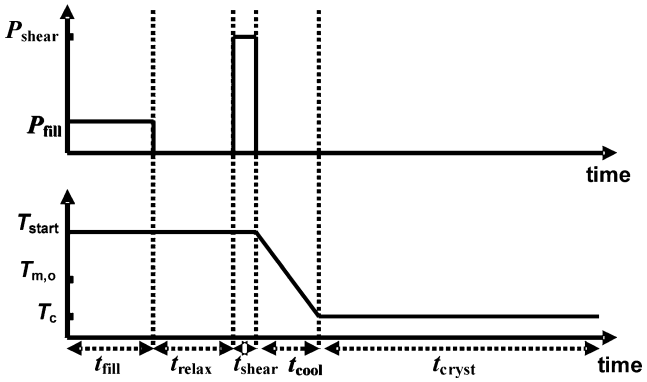


**Fig. 1** Scheme of the melt memory protocol used in this work for the isothermal experiments. The shear pulse is applied at the processing temperature and the sheared melt is immediately cooled to the crystallization temperature. Recording of crystallization kinetics is performed in the absence of flow. Reprinted with permission from [14] (copyright 2005, American Institute of Physics [9])

This is therefore the reason why we call this protocol "the melt memory protocol".

The philosophy behind the melt memory protocol is also different from that followed by other apparently similar experimental setups used to study the effect of shear flow on the enhancement of crystallization kinetics, which are mainly based on the "short-term" shearing protocol [11]. With this protocol, the enhancement of crystallization kinetics resulted from the application of shear deformations at the crystallization temperature. One problem with this protocol is the lack of control of strain applied to the polymer pumped from the accumulator to the duct. Depending on the shear pulse time duration and intensity, the hotter melt is pumped from the accumulator (at $T > T_m$) to the duct (at $T = T_c$) in short time intervals, which are followed by relatively long time intervals for recording the crystallization. Therefore, the melt at the accumulator may relax fully or that relaxation may be incomplete. This lack of melt deformation control inhibits the use of "short-term" shearing protocol to study the origin of melt memory effect. The strain applied to the melt is also limited by the length of the duct (around 100 s.u.). The shear DTA device enables applying to the melt controlled deformation values, similar to those previously used by Chai et al. [7].

### Rheological experiments

All rheometer experiments were performed in a Physica MCR 300 rheometer (Paar Physica) with parallel plate configurations (25 mm in diameter). The gap was set to 0.7 mm for all experiments. Controlled shear rate experiments (CSR) were performed between 140 and 170 °C for ZNPE and between 140 and 180 °C for MPE. The constant stress used in the above temperature range for experiments with both polymers at the viscoelastic linear regime was 1,000 Pa. Small-amplitude oscillatory shear experiments were performed between 130 and 170 °C for ZNPE and between 140 and 170 °C for MPE. Shear stress growth experiments were performed between 150 and 170 °C for ZNPE and between 180 and 200 °C for MPE. The reason for using so high a temperature range for the shear stress growth experiments resulted from the need to detect the attainment of steady state. For the sheared melt, it occurs after a relatively long time and it decreases by increasing the sheared melt temperature.

## Results

### Crystallization kinetics after pre-shear

The results described below were obtained following the melt memory protocol (Fig. 1). We started the crystallization experiments with a relaxed melt that was obtained by pumping material from the accumulator to the capillary channel with low shear rates, closing the upper and lower valve of the capillary and maintaining the polymer stored in the capillary at a temperature above the equilibrium melting temperature for a period longer than 30 min. After this annealing period, the polymer was cooled to the crystallization temperature and crystallization kinetics was recorded by measuring the temperature difference between the sample at the capillary and a reference (empty) capillary channel. Figure 2 shows the results obtained for the melt at 240 °C and crystallization temperature of 115 °C. The solid line is the result obtained for relaxed melts. It is visible that ZNPE has faster crystallization kinetics than MPE.

Scanning electron microscopy (SEM) was used to evaluate the morphology of samples crystallized in a DSC following a similar temperature program as in Fig. 2. The results shown in the supplementary information indicate that ZNPE has a lower nucleation density than MPE. Its average spherulite diameter is around 70 μm and that of MPE is around 8 μm. The corresponding average nucleation density is $5.57 \times 10^{12}$ nuclei/m$^3$ and $3.73 \times 10^{15}$ nuclei/m$^3$ for ZNPE and MPE, respectively.

The MPE spherulite radius ($R_0$=4 μm) agrees with the value obtained by Chai et al. [7] ($R_0$=3 μm), which is not surprising since the molecular weight and the molecular weight distribution of the polymers used are similar. Since the applied deformation and cooling rate used by Chai et al. are similar for metallocene and Ziegler–Natta polyethylenes, the relative difference in their corresponding final spherulite sizes agrees with the relative difference in the spherulite radius for the polyethylene samples used in this work.

The surprising results of these experiments are the faster crystallization kinetics of ZNPE and the factor(s) responsi-

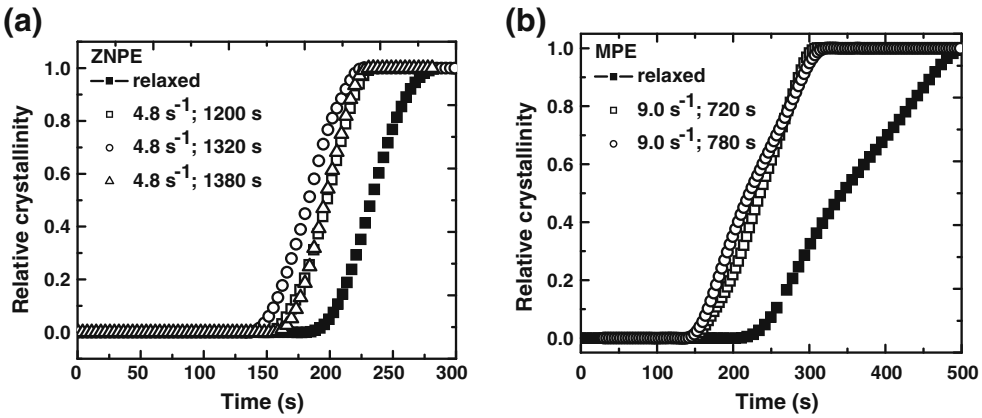


**Fig. 2** Isothermal crystallization of polyethylene Ziegler–Natta (**a**) and metallocene (**b**) recorded with shear DTA: $T_c$=115 °C, $T_m$= 240 °C, constant shear rate of 4.8 $s^{-1}$ for ZNPE and 9.0 $s^{-1}$ for MPE, shearing times indicated. The average critical strain for ZNPE is 5,760 s.u. and 6,480 s. u. for MPE

ble for its lower nucleation density when compared to the MPE sample's results. In principle, one would expect an opposite behaviour to that reported above, namely, that crystallization kinetics would be fastest for the polymer with a higher nucleation density. One factor that may explain the fastest crystallization kinetics of ZNPE is its higher equilibrium melting temperature and consequently higher supercooling degree. Because nucleation densities were estimated for samples crystallized at the same temperature, the supercooling degree is ≈2.2 °C higher for the ZNPE sample (see Table 1). However, as shown below, this effect alone cannot explain the different half-crystallization time of relaxed melts crystallized at the same temperature.

In Avrami's formalism, the half-crystallization time may be expressed as a function of the average nucleation density $\overline{N}$ and the spherulite growth rate $G$:

$$\left(\frac{1}{t_{50\%}}\right) = \ln(2)^{-1/3} \cdot \left(\frac{4\pi}{3}\frac{\rho_s}{\rho_l}\right)^{1/3} \cdot (N)^{1/3} \cdot G = \alpha \cdot \left(\overline{N}\right)^{1/3} \cdot G, \tag{1}$$

where $\rho_s$ and $\rho_l$ are the solid and liquid phase densities, respectively, and $\alpha = \ln(2)^{-1/3} \cdot (4\pi\rho_s/3\rho_l)^{1/3}$.

The ratio of the reciprocal half-crystallization time of MPE ($m$) and ZNPE (zn) for relaxed melts crystallizing at the same temperature is

$$\frac{(t_{50\%})_m}{(t_{50\%})_{zn}} = \frac{\left(\overline{N}_{zn}\right)^{1/3} \cdot G_{zn}}{\left(\overline{N}_m\right)^{1/3} \cdot G_m} = \frac{\left(\overline{N}_{zn}\right)^{1/3} \cdot \exp\left(-\Delta G_{d,zn}/RT\right) \cdot \exp\left(-k_g/T \cdot \Delta T_{zn} \cdot f\right)}{\left(\overline{N}_m\right)^{1/3} \cdot \exp\left(-\Delta G_{d,m}/RT\right) \cdot \exp\left(-k_g/T \cdot \Delta T_m \cdot f\right)}, \tag{2}$$

We have considered in Eqs. 1 and 2 an instantaneous nucleation of spheres and the spherulite growth rate was expressed by the Laurizten and Hoffmann general equation, with $\Delta G_d$ representing the activation energy for transport of chain stems to the spherulite growth front, $\Delta T$ the supercooling degree, $f$ the factor accounting for the variation of the enthalpy of fusion with temperature and $k_g \propto \sigma \cdot \sigma_e / \Delta h_f^0$; $\sigma$ and $\sigma_e$ are the lateral and fold surface free energy, respectively, and $\Delta h_f^0$ is the enthalpy of fusion of the perfect crystal.

The measured half-crystallization time for the relaxed melts of MPE and ZNPE is 345 and 231 s, respectively. To estimate the effect of different supercooling degrees on the faster crystallization kinetics of ZNPE, we may consider similar $k_g$ values for both polymers ($1.24\times10^5$ $K^{-2}$) and that their activation energy for the transport of chain stems to the lamellae growth front are also similar. Considering the values evaluated above for the nucleation density of ZNPE and MPE, we have from Eq. 2: $t_{50\%,m}/t_{50\%,zn} = 3.62$, while the value evaluated from the experiments of Fig. 2 is $t_{50\%,m}/t_{50\%,zn} = 1.49$. This difference between the estimated and experimental results suggests that $\Delta G_d$ should be different for the two polymers and that it should play a significant role on the crystallization kinetics development. We return to this issue in the "Discussion" section.

Going back to the results of Fig. 2, we see that the application of shear deformations to the melt, at temperatures above their equilibrium melting temperature, accelerates the crystallization kinetics until saturation, which is reached after shearing the melt with large strain values. By saturation, we mean that further melt deformation has no effect on the crystallization kinetics. This observation is similar to that reported by Chai et al. for the crystallization from pre-sheared ZNPE melts [7]. The results of these experiments were obtained by applying constant shear rates, 4.8 and 9 $s^{-1}$ for ZNPE and MPE, respectively, and different shearing times. Similar strain values at saturation

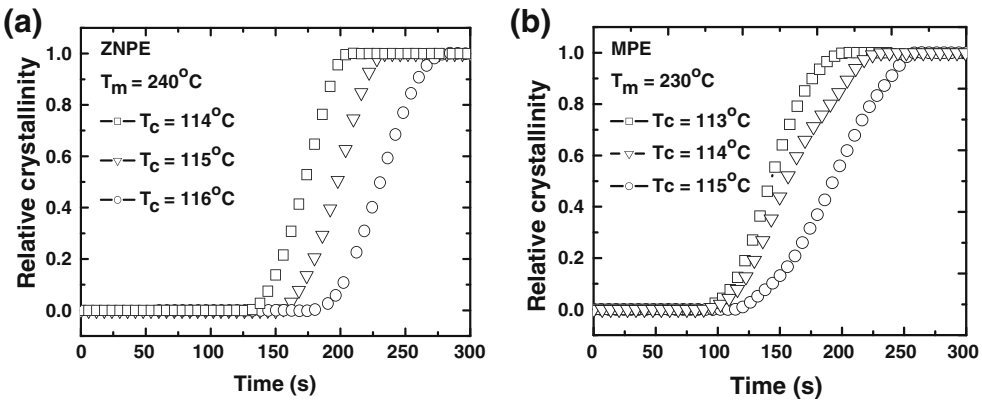


**Fig. 3** Effect of crystallization temperature on the saturation of crystallization. Constant shearing temperatures (240 °C for ZNPE and 230 °C for MPE) and shear rate (4.8 $s^{-1}$ for ZNPE and 7.6 $s^{-1}$ for MPE) at different crystallization temperatures for ZNPE (**a**) and MPE (**b**). The average critical strain for ZNPE is 5,760 s.u. and for MPE is 6,840 s.u.. The measurement error of strain is ±15% around the mean

are obtained if the melt is sheared at different shear rates during constant shearing time (results not shown) [6, 8, 15].

Figure 3 provides a further demonstration that strain is the factor behind the acceleration of crystallization and its saturation. These results refer to crystallizations from the same melt temperature and different crystallization temperatures for ZNPE, Fig. 3a, and MPE, Fig. 3b. For simplicity, this figure and the others show only the saturated crystallization kinetics results. Regardless of the crystallization temperature, the strain needed to saturate crystallization is the same. In this case, the different kinetics results only from the supercooling degree effect on crystallization.

The data of Figs. 2 and 3 suggest that the saturation of crystallization kinetics results from a melt effect, implying that a well-defined melt state should be responsible for this behaviour. Therefore, the information of strain variation with melt temperature could provide information that would allow us to identify that melt state. This information was obtained by shearing the melt at different temperatures and recording the crystallization at a constant temperature. In this way, any effect on crystallization kinetics resulting from the different supercooling degrees, or nucleating agents, is eliminated. The only effect recorded is the melt ability to store the memory of a previous flow history.

Figure 4 shows the results of these experiments for ZNPE. The strain that saturates crystallization decreases with sheared melt temperature increase and crystallization kinetics is almost independent of the sheared melt temperature. Similar results were obtained for other polymers [6, 8].

## Identification of the melt state responsible for the saturation of crystallization

As mentioned above, the results of Figs. 2, 3 and 4 suggest that the attainment of a well-defined melt state should explain the behaviour observed. To identify this state, we performed similar experiments in a rheometer by measuring the viscosity (or shear stress) variation with time at a constant shear rate.

Figure 5a, b show the results of shear stress growth experiments for ZNPE and MPE, respectively. The variation of viscosity (or shear stress) with time, at a constant shear rate, initially increases, passes through a maximum (the yield stress) at low strain values, decreases and finally stabilizes with a constant value at the steady state. The strain at the yield stress marks the onset of chain disentanglement that reaches a stable value at steady state. While for some polymers and shear rates it is possible to obtain a well-defined steady state [6, 8], this was not the case for the materials used in this work.

Figure 5 demonstrates the difficulty in the definition of the onset of steady state. This difficulty arises from polymer thermal degradation—which is a problem to be considered at high melt temperatures—the mass loss of polymer between plates, among other effects, that affect the accuracy with which strain values at the onset of steady state are evaluated. For these reasons, these experiments were repeated several times (at least four times for each temperature and shear rate) and they were performed with nitrogen flow. The strain values indicated in Fig. 5a, b correspond to an experiment within the average of the measurements performed.

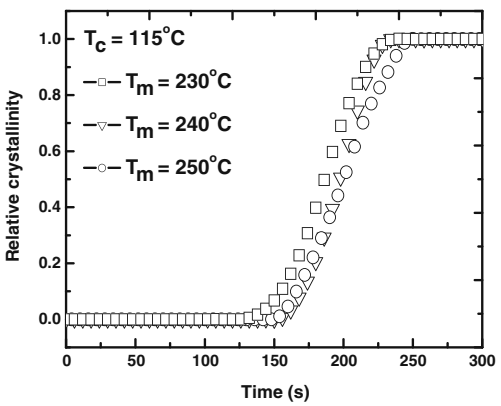


**Fig. 4** Effect of the sheared melt temperature on the saturation of crystallization of ZNPE. Constant crystallization temperature (115 °C) and shear rate of 4.8 $s^{-1}$ at different melt temperatures: 230 °C, $\gamma_c$= 5,929 s.u.; 240 °C, $\gamma_c$=5,760 s.u.; and 250 °C, $\gamma_c$=5,508 s.u

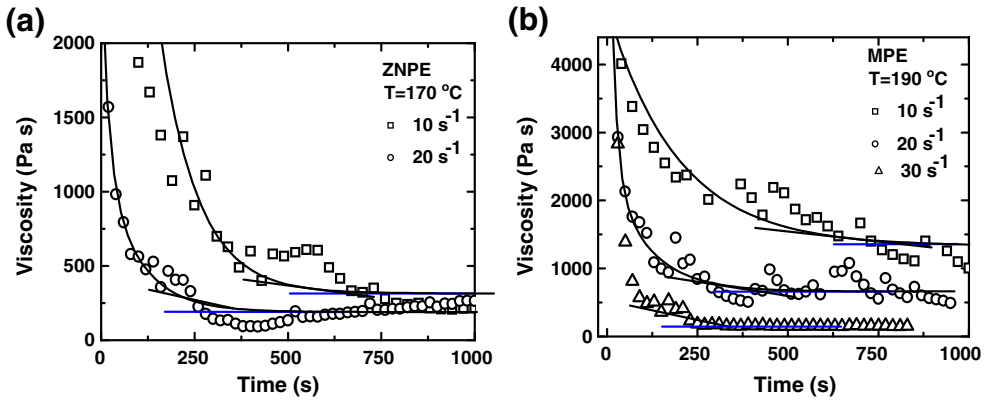


**Fig. 5** Transient viscosity as a function of time in stress growth experiments performed at 170 °C for ZNPE (**a**) and at 190 °C for MPE (**b**). The *solid lines* show the procedure used to evaluate the critical strain at the onset of steady state. For ZNPE, the average critical strain is 7,230 s.u. (±562)—6,700 s.u. for 10 $s^{-1}$ and 7,760 s.u. for 20 $s^{-1}$. For MPE, the average critical strain is 9,330 s.u. (±1,364), 9,070 for 10 $s^{-1}$, 8,300 s.u. for 20 $s^{-1}$ and 10,620 s.u. for 30 $s^{-1}$

The experimental curves were fitted with a single exponential decay function and the onset of steady state was evaluated at the intersection point of a tangent line to the plateau where viscosity changes by more than 10% of the plateau value. This variation is assigned by the instrument manufacturer as the accepted viscosity measurement error. The measurement error of this strain is 15% of the mean value.

We wish to stress that the results of Fig. 5, which were obtained with a different instrument, did not only validate the shear DTA experimental results (Fig. 6), since they yield similar strain values at the onset of steady state with similar temperature variation, but also demonstrate clearly that steady state is the melt state responsible for the saturation of the crystallization kinetics of melts sheared above their melting temperature. These results agree with those of previous works for polyethylene and polypropylene melts [6, 8].

Understanding the melt morphology at steady state is, in our view, essential to explain the reasons behind the saturation of crystallization kinetics in melts crystallized under quiescent conditions that keep the memory of flow deformation previously applied above their melting temperature. To gain further insight into this morphology, we performed small-amplitude oscillatory shear experiments at the constant stress of 1,000 Pa for melts of ZNPE and MPE. The results of these experiments at different temperatures allowed us to evaluate the relaxation time at the crossing point of $G'(\omega)$ and $G''(\omega)$ and the flow activation energy. Figure 7 shows the reduced curves obtained for both polymers at the reference temperature of 160 °C. Additional information for these results can be found in Fig. SI.4a–c in the supplemental information. The relaxation time at 160 °C is also indicated in Fig. 7. We consider it as the reptation time and its temperature variation is presented in Fig. 6.

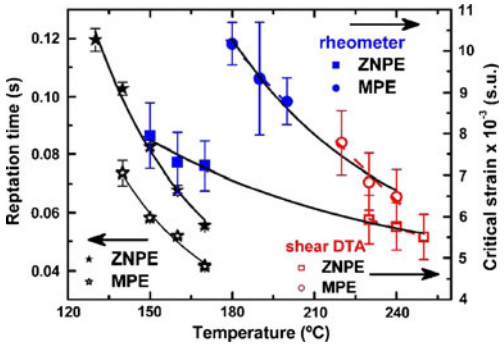


**Fig. 6** Temperature variation of the reptation time (*stars*) and critical strain (*circles* and *squares*) for ZNPE and MPE. The critical strain measured with the shear DTA (*open circles* and *squares*) and in shear–stress growth experiments with parallel plate (*filled circles* and *squares*) is plotted as a function of sheared melt temperature: *squares* represent ZNPE and *circles* MPE. The experimental errors of measurements are indicated by *error bars*. *Data points* represent the average values of measurements. Values of reptation time for melts sheared up to the steady state are expected to be around half the values indicated

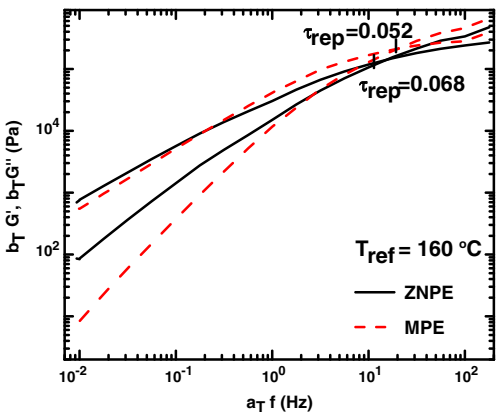


**Fig. 7** Reduced curves of small-amplitude oscillatory shear experiments for Ziegler–Natta and metallocene polyethylene at the reference temperature of 160 °C

These last values were evaluated only for relaxed melts where pre-shear effects, or melt memory effects due to previous flow deformations, were eliminated by annealing of the melt. ZNPE has a slightly higher reptation time than MPE, which may be explained by its higher polydispersity and higher values of $M_w$ and $M_z$.

Additional information for the melt morphology at steady state was obtained from small-amplitude oscillatory shear experiments performed in melts sheared up to the steady state [6, 8]. Polyethylene melts were pre-sheared with constant shear rate up to the steady state following the procedure used to obtain the results of Fig. 5. Then, small-amplitude oscillatory shear experiments were performed with the same constant stress used for relaxed melts. It was shown—Fig. SI.3 in the supplemental information—that relaxed polyethylene melts, when sheared up to the steady state, loose around one half of the initial entanglements. In different words, the melt state responsible for the saturation of crystallization is a partially disentangled melt. However, the flow activation energy of relaxed melts and melts sheared up to the steady state are similar. In agreement with literature results [3], it was found that the flow activation energy of MPE is higher than that of ZNPE (see Table 2).

**Table 2** Flow activation energy of ZNPE and MPE

| PE | $E_a$ (kJ/mol) | |
|---|---|---|
| | SAOS | CSR |
| ZN | 24.46±1.53 | – |
| M | 29.93±1.21 | 26.38±3.00 |

## Discussion

### Effect of flow memory effect on the quiescent crystallization kinetics of MPE

The results of Figs. 2, 4, 5 and 6 contradict those of previously published works which suggested "any significant influence of melt pre-shear on the subsequent crystallization of metallocene polyethylene" [7]. This interpretation was explained by the absence of long chains in the metallocene based-polymer and the fast molecular disorganization at the end of flow, leading to a lack of flow memory effect on crystallization.

The results of Fig. 7 demonstrate that both polymers, ZNPE and MPE, have similar reptation time, although $\tau_{ZNPE}$ is slightly higher than $\tau_{MPE}$. Despite differences in their molecular weight distribution, the experimental curves of $G'(\omega)$ and $G''(\omega)$ cross at a similar frequency value. Because of their similar longest relaxation time, it is expected that any pre-shear deformation should manifest in a similar way.

In fact, the flow memory effect on crystallization is present in crystallizations from pre-sheared melts of both ZNPE and MPE, but metallocene polyethylene requires a larger strain to reach the steady state and to saturate the crystallization. This may be the reason for the conclusion of Chai et al. [7] that pre-shear has no significant influence on the crystallization of metallocene polyethylene. In agreement with Chai et al., large strains are needed to establish a steady state in shear flow and saturate the solid-state morphology developed from melts sheared up to this state.

### Validity of experimental results

Before continuing this discussion, we proceed with a detailed analysis of the experimental results validity. The first issue to address is polymer degradation. This problem is in principle absent in the experiments performed with the shear DTA instrument since the melt is enclosed by the capillary channels and do not have contact with air. We checked this assessment by performing repeated crystallization experiments, which are reproducible within the experimental measurement errors [6]. Additionally, the results obtained with this instrument were compared with those obtained with a rheometer. Figure 8 provides additional confirmation of the absence of this effect on the results obtained. It shows reversibility on the effects of slowing down and acceleration of crystallization kinetics.

As for the results obtained with the rheometer, it was shown that for materials for which it was possible to perform shear DTA and rheometer results at the same temperature, similar strain values were obtained in the two different instruments for saturating the crystallization and establishing a steady state. A more complete and detailed discussion of the validity of these results may be found in [6]. Further, results similar to those we have obtained, with well-defined steady state, were obtained in 1980 for polyethylene by Wagner and Meissner [16] where a cone-and-plate configuration was used—see also [8].

We discuss next the need for large strain values to saturate crystallization, which agree in magnitude with those obtained by Chai et al. [7] and also with independent results obtained through a rheometer with parallel and cone-and-plate configurations [8]. This strain is also independent of the shear DTA capillary diameter. Similar strain values at the onset of steady state were obtained in rheometer experiments performed with plates of different diameters (25 and 40 mm). Further, these results agree with others obtained with the cone-and-plate configuration, which are two third lower than those evaluated with the parallel plate configuration. The unique reason for this difference is that the average shear rate in experiments with parallel plate configuration is two third the value at the edge

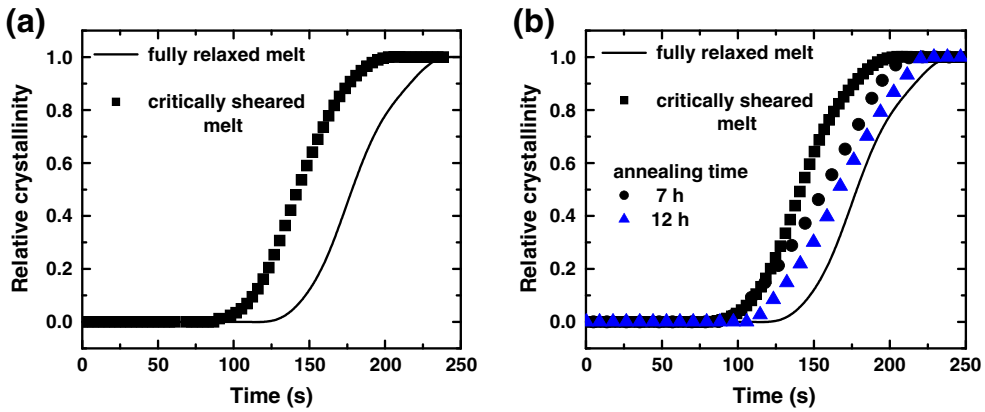


**Fig. 8** Acceleration (**a**) and slowing down (**b**) of crystallization kinetics in a melt of MPE at 230 °C. The crystallization temperature is 113 °C. **a** *Solid line* represents crystallization of the relaxed melt and *filled squares* represent the saturation of crystallization at 6,970 s.u. **b** Melts sheared up to the steady state with the strain of around 7,000 s. u. (*filled squares*) were annealed, before crystallization, during different times. Crystallization of a relaxed melt (*solid line*) is obtained again after annealing of around 12 h (*triangles*)

of the plate [6]. The agreement between the results obtained with these two configurations excludes slippage of polymer between plates as a possible source of error and guarantees a laminar flow at steady state. Also, the suggested possible bonding of polymer chains to the metal surfaces of capillary channel, or to the rheometer plates, playing the role of grafted chains [17], acting as a lubricant and promoting chain slippage, is excluded based on the above results obtained with the parallel plate and cone-and-plate configurations.

The results of Fig. 2 (or Figs. 3 and 4) cannot be assigned also to the presence of impurities, nucleating agents or additives present in the commercial polymer sample used, such as those described, for example, by Byelov, Panine and de Jeu [18]. The same melt and crystallization temperatures were used in these experiments. The only variable was the strain applied to the melt. The concentration of nucleating agents and the exposure of their surfaces to the melt are the same in all experiments.

Still another possible source of error is the increase of equilibrium melting temperature, and therefore supercooling degree, due to pressure increase originated by flow. Because crystallization occurs in the absence of flow and since only the memory of flow deformation effects is studied, it is expected that the effect of pressure on the quiescent melt at the capillary relaxes within a time comparable to the longest relaxation time. Also, since no pressure was applied to the polymer during its crystallization, there is no change of equilibrium melting temperature to consider.

## Erasing the pre-sheared melt memory by annealing of the melt

With the above discussion, we expect to have clarified doubts concerning the validity of the experimental results obtained. To further testify their validity, the melt sheared up to the steady state was annealed during different time intervals. Figure 8a shows the crystallization kinetics of the polymer melt cooled from two well-defined melt states: the relaxed (fully entangled) melt and critically sheared (partially disentangled) melt. The result of annealing the critically sheared melt is presented in Fig. 8b. The same melt and crystallization temperatures were used for these experiments, 230 and 113 °C, respectively. Increasing the annealing time slows down the crystallization kinetics until the recorded crystallization kinetics is again similar to that of a fully entangled melt (after an annealing of around 12 h). These results demonstrate the possibility of erasing the flow-induced melt memory by annealing of the melt.

Before proceeding on with an analysis of results, we note that they are similar to those previously reported by Chai et al. [7] for the effect of waiting time on the melt memory. They also demonstrate that critically sheared melts store the memory of flow deformation for a time much longer than the longest relaxation time. This effect cannot result from the relaxation of chain orientation with the flow direction since any chain orientation induced by flow relaxes faster than the longest relaxation time. The following argument supports the above assessment. At 160 °C, the longest relaxation time for these polymers is around $10^{-2}$ s. Any orientation induced to the chains by flow relaxes within the Rouse relaxation time of the chain, around $1.07\times10^{-5}$ s. This value is obtained after the following reasoning. The chain diffusion coefficient is $k_BT/\zeta_{chain}$, with $\zeta_{chain} = N_k\zeta_k$, where $\zeta_k$ is the Kuhn monomer friction coefficient, equal to $4.74\times10^{-13}$ kg/s for PE (estimated at $T$=463 K) [19]. The chain with a molecular weight of 100,000 g/mol contains around 667 Kuhn monomers and $D_{chain}$ is then $2.02\times10^{-11}$ m$^2$/s. The PE Kuhn monomer length is 14 Å, and the Rouse

relaxation time of the chain is approximately $\tau_R = \langle [r(t) - r(0)]^2 \rangle / 6D_{chain} \approx 1.07 \times 10^{-5}$s. We therefore need to consider a relaxation time much longer than the longest relaxation time to explain the melt memory.

The effects of chain stretching and chain retraction are not considered relevant for the melt memory effect since they occur for fast flows at a rate comparable to the reciprocal of the Rouse relaxation time of the chain. The melt memory persist for a time orders of magnitude higher the Rouse relaxation time of the chain. Although these two effects may compete for the formation of the disentangled melt state, it was proposed by Marrucci [20] that they cancel each other: while chain retraction contributes to increasing the tube diameter, chain stretching contributes to its decrease in the same amount [21].

## Melt memory effect

As stated by de Gennes: "some strange things happen in polymer melts for times longer than the terminal time (reptation time). Memory effects are present for many hours in samples where the terminal time is smaller than 1 min" [22]. Of importance to this work is the effect of melt memory on polymer crystallization. Results of works published so far suggest that we should consider two different contributions for the melt memory effect on polymer crystallization. One contribution may be classified as a *thermal melt memory effect* and the other as a *flow-induced melt memory effect*. The former accounts for contributions to the melt memory resulting from heterogeneities present in the sample, effects of contact with the walls of the container and eventual mesophases present in the polymer melt [23, 24]. The later is related to changes in the melt morphology induced by the rotational and elongational components of shear flow and the effect of these changes on the melt solidification behaviour [25, 26]. We may include in this last effect the so-called shear-induced precursor structures since they result from flow deformations applied to a relaxed melt.

The shear-induced precursor structures have been linked to the formation of an oriented surface layer on the extruded sample that appears when the extruded melt is quenched and is absent when the melt is maintained for a certain time at the extrusion temperature [25, 26]. This last result is similar to that described in Fig. 8b. However, in these experiments, crystallization occurred concurrently with shearing of the melt. A representation of the zero shear rate viscosity at a melt temperature versus the relaxation time for the decay of birefringence in the oriented layer at the same melt temperature allowed the authors to conclude that the precursor structures are too thin to affect melt rheology (because the slope of the line connecting the experimental data is lower than 1) [25, 26]. Our work shows, as demonstrated below, that the disentangled melt rheology, namely, its lower viscosity, affects strongly the crystallization kinetics. We reached this conclusion because in this work we separate the deformation of the melt that occurs only at the processing temperature from its crystallization which occurs in the absence of flow. We pretended to understand the ability of the melt to store the memory of flow deformations, which is necessarily related to the melt morphology and its change by flow.

## Role of "tight" knots

It was considered by de Gennes [22] that this ability results from tight knots that were viewed as very stable, persisting for a long time after heating the sample above its melting temperature. Whatever the geometry considered for the knot, the interaction energy for the participating chain segments at the knot may always be evaluated. "Very stable" arrangements imply an interaction energy higher than the melt thermal energy.

A good representation of a knot is a loop with a chain at its centre. It was shown that the interaction energy involved is given by [27]:

$$W_l \cong -\frac{3\pi C L_l}{8\lambda^2 R^5}, \tag{3}$$

where $R$ is the radius of the loop, $\lambda$ is the separation distance between two consecutive units of the chain or loop, $L_l$ the length of the loop and $C$ is the London constant, which is related to the number density of molecules in the chain ($\rho$) and Hamaker constant ($A$) by $A=\pi^2\rho_1\rho_2 C$. For polyethylene, $\lambda$=1.26 Å, $R$=4.80 Å, $L_l$= 30.2 Å and $C = 5.64 \times 10^{-79}$Jm$^6$ at 200 °C. With these values, $W_l$=3.0 kJ mol$^{-1}$ while the thermal energy is 3.9 kJ mol$^{-1}$. This evaluation demonstrates that the "tight knots" between polymer chains cannot explain the melt elasticity and the origin of flow-induced melt memory recorded with the experiments described above [27, 28] and it asks for a new definition of the interaction between the chain segments responsible for the effects assigned to entanglements.

To understand that origin, it is important to answer the question: what are the physical mechanisms behind the acceleration of crystallization kinetics with the increase of shear strain and its slowing down by annealing of the melt? Without entering into details about the melt morphology, its change with shear flow and the physical nature of entanglements, we can analyse the growth rate of spherulites in fully entangled and disentangled melts, study its variation with the crystallization temperature and measure the final size of spherulites crystallized from fully entangled and partially disentangled melts.

## Possible physical explanation for the acceleration of crystallization kinetics in pre-sheared melts and its slowing down by annealing of the melt

### *The decrease of viscosity in disentangled melts*

The experimental results obtained by different groups of authors demonstrated that the application of shear implies a decrease in the number of entanglements, although the final number of entanglements after the application of shear was not evaluated. Exceptions are the works in [6, 8]. It is known that the repeated extrusion of low-density polyethylene leads to "shear refining", which is a decrease in the viscosity of the melt. Annealing the "shear-refined" melt at 160 °C for a period of 2 h leads to the reverse effect, an increase of viscosity [10]. Due to the similarity of these experimental results and those presented in this work, it appears that the lower melt viscosity of critically sheared melts could explain their faster crystallization kinetics.

In crystallization experiments, melt viscosity is linked also to the ability of chains moving to the lamellae growth front, affecting both the nucleation and growth rate—therefore the overall crystallization kinetics. This link is discussed further in the following paragraphs.

### *Role of the spherulite growth rate*

However, faster crystallization kinetics could result also from different nucleation densities and different growth rates. Experimental results for the spherulite growth rate in fully entangled and disentangled melts were obtained by Psarski et al. [29]. The disentangled melt was obtained by the application of high pressure to polyethylene. Under this condition, polyethylene crystallizes in the form of extended chains. Results of Fig. 9 from [29] show the effect of annealing time on the spherulite growth rate of fully entangled melts (which is constant) and disentangled melts (decreasing with annealing time). In agreement with the results of Fig. 8, annealing of the melt slows down the crystallization kinetics. Spherulites of disentangled melts grow faster by about 25% to 45%, and after an annealing time of around 30 min the growth rate is comparable again with that of a fully entangled melt.

To check if the different growth rate is the only factor behind the faster crystallization kinetics of partially disentangled melts or if crystallization from these melts also yields a different nucleation density, we analyse further the crystallization of MPE at 113 °C as shown in Fig. 8a. The half-crystallization time is 143 s and 178 s for critically sheared and relaxed melts, respectively. The ratio $t_{50\%,rel}/t_{50\%,sh}$ should be equal to $G_{sh}/G_{rel}$ if the growth rate was the only factor behind the faster crystallization kinetics of pre-sheared melts. The ratio between the half-crystallization times we have measured is 1.24, while that of the $G_{sh}/G_{rel}$ evaluated from the data of Fig. 9 is 1.4. Although these values are similar, they are not directly comparable since they were evaluated with different polyethylene samples and the procedure used by Psarski et al. to obtain the disentangled melt state was also different than the one used in the present work. We conclude for now that the different spherulite growth rate plays an important contribution in the faster crystallization kinetics of disentangled melts. However, the dominant role on this faster growth rate may result from the surface nucleation of chain stems or from their transport to the lamellae growth front. This issue is discussed further in the section "Role of the chain diffusion to the lamellae growth front".

### *Role of the nucleation density*

The results of Fig. 10 obtained with MPE samples crystallized from relaxed and critically shared melts indicate that the former yields spherulites with a larger diameter, 4.70 and 4.25 μm, respectively. This evaluation was made with small-angle light scattering experiments on 100-μm sections cut from samples crystallized by cooling the melt from 220 °C with a constant cooling rate of −5 °C/min. The $H_v$ pattern obtained allowed the evaluation of the intensity variation at 45º to the vertical which is represented as the ordinate in Fig. 10. The abscissa was evaluated for each experimental data point of the intensity by $R = 4\lambda/4\pi\sin(\theta)$, where $\lambda$ is the wavelength (632.8 nm) and $\tan^{-1}\theta = x/d$, where $d$ is the distance from the sample to the detector and $x$ is a data point along the line drawn at 45º. The average spherulite radius corresponds to the maximum value of $R$.

The nucleation densities corresponding to the above spherulite radius are $2.30\times10^{15}$ nuclei/m$^3$ and $3.11\times10^{15}$ nuclei/m$^3$, respectively. As can be seen in Fig. SI.5 and similarly to results presented in another work [9], the

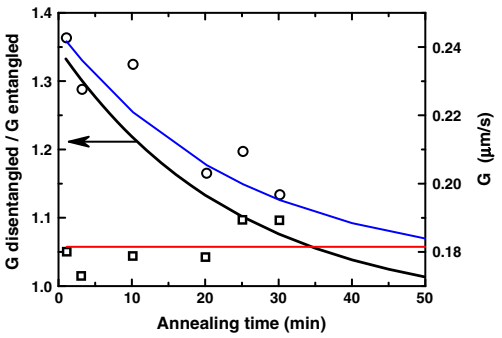


**Fig. 9** Effect of the annealing time at the melt temperature of 160 °C on the crystallization of polyethylene at 123 °C for fully entangled melts (*squares*) and disentangled melts (*circles*). Experimental data from Psarski et al. [29]

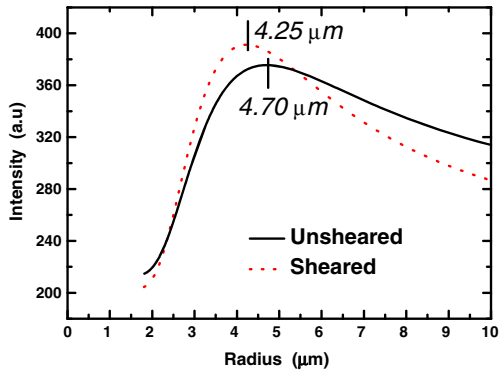


**Fig. 10** Average spherulite radius of MPE evaluated by small-angle light scattering. The samples were crystallized by cooling the melt from 200 °C with a constant cooling rate of −10 °C/min. The *solid line* is the result obtained for an unsheared (fully entangled) melt and the *dotted line* corresponds to a partially disentangled sample sheared up to the steady state with the strain of 9,000 s.u.

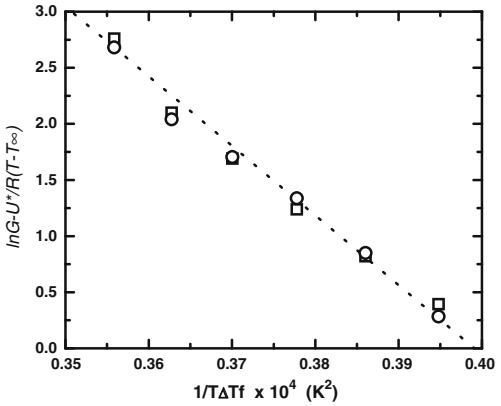


**Fig. 11** Representation of experimental results obtained by Huo et al. for the spherulite growth rate of fully entangled (relaxed) iPP melts cooled from 200 °C (*squares*) and melts sheared at this temperature during 10 min with the shear rate of 5 $s^{-1}$ before the isothermal crystallization. The slope of the curve is similar for crystallizations from the two melt states: $k_{G,\text{relaxed}} = -6.27 \times 10^5 \text{K}^{-2}$ and $k_{G,\text{sheared}} = -6.20 \times 10^5 \text{K}-^2$. Data were extracted from Figs. 3 and 4 of [30]

morphology is spherulitic for both samples, fully relaxed and disentangled. Since for an instantaneous nucleation of spheres $t_{50\%,\text{rel}}/t_{50\%,\text{sh}}$ is proportional to $\left(\overline{N}_{\text{sh}}/\overline{N}_{\text{rel}}\right)^{1/3}$, we may estimate the role of different nucleation density on crystallization kinetics. The ratio $\left(\overline{N}_{\text{sh}}/\overline{N}_{\text{rel}}\right)^{1/3}$ is 1.11, which is below the value of 1.24 evaluated for the ratio between the two half-crystallization times. We conclude then that a different nucleation density represents a small contribution for explaining the faster crystallization kinetics of pre-sheared melts. We note that the samples used to evaluate the spherulite dimensions were prepared in a parallel plate rheometer and their crystallization conditions are different from those used in the shear DTA instrument. The reason was the lack of physical possibility of extracting samples from the shear DTA instrument for morphological analysis. Despite the different crystallization conditions, it is reasonable to assume that the ratio between the nucleation densities is comparable with that between the half-crystallization times because melts were cooled from the same temperature and sheared until the attainment of a steady state.

### *Role of the chain diffusion to the lamellae growth front*

Since growth rate depends on the melt viscosity via the diffusion term for the transport of chain stems to the spherulite growth front and on the secondary nucleation at the lamellae surface, it is important to ascertain which of these two contributions, and to what extent, is affected by the different density of entanglements. The results obtained by Huo et al. [30] clarified this issue.

Figure 11 shows the logarithm of the growth rate as a function of $1/T\Delta Tf$ for crystallizations from relaxed melts at 200 °C and melts sheared at 200 °C during 10 min with the shear rate of 5 $s^{-1}$ (strain 3,000 s.u., similar to that used in our experiments). The data used for the different parameters were extracted from [30]. Similar slopes were obtained for crystallizations from these two different melt states. These results demonstrate a small, or negligible, effect of secondary crystallization in the different growth rate from fully entangled and critically sheared melts. By exclusion, it remains then the additional contribution of the diffusion term, and the lower viscosity of sheared melts, to explain the faster growth rate and the flow-induced melt memory effect.

## Conclusions

One goal of this work was to verify the impossibility of the enhancement and saturation of crystallization kinetics for metallocene-based polyethylene presented in literature and to establish the origin of melt memory effect observed in the crystallization of polymers obtained with different catalysts. It is concluded that metallocene-based polyethylene behaves in a way similar to any other linear polymer chains. Controlled shear deformations applied above the equilibrium melting temperature enhances crystallization kinetics until saturation. The strain required to achieve saturation decreases by increasing the melt temperature. This saturation was found to occur at higher critical strains for metallocene polyethylene compared to Ziegler–Natta polyethylene.

Our results do not differ too much from those of Chai et al. [7] with the exception that we also found the saturation of crystallization in metallocene-based polyethylene at larger strain values than those observed for ZNPE. In

agreement with their results for ZNPE, we demonstrate also that increasing the waiting time (annealing time) at the melt temperature after shear slows down the crystallization kinetics. After an annealing time of 12 h, the kinetics becomes comparable to that of a relaxed melt. This annealing process erases the shear-induced melt memory, increasing the viscosity of the melt due to the rebuild-up of the entanglement network [20].

The faster crystallization kinetics of disentangled melts results from their lower viscosity that affects the transport of chain stems to the lamellae growth front, hence the spherulite growth rate. On the contrary, annealing the disentangled melt increases its viscosity, rebuilding the original entanglement "network" and slowing down the crystallization kinetics.

**Acknowledgments** We thank Choon K. Chai for supplying us the materials used in these experiments, Andrzej Galeski for the NMR and SEM experiments and the Portuguese Foundation of Science and Technology for funding the projects FCOMP-01-0124-FEDER-007151 (PTDC/CTM/68614/2006). This work was supported by the European Community fund FEDER and project 3599/PPCDT.

## References

1. Sinn H, Kaminsky W (1980) Adv Organomet Chem 18:99–149
2. Wang C, Chu M-C, Lin T-L, Lai S-M, Shih H-H, Yang J-C (2001) Polymer 42:1733–1741
3. Gelfer M, Horst RH, Winter HH, Heintz AM, Hsu SL (2003) Polymer 44:2363–2371
4. Rastogi S, Lippits DR, Peters GWM, Graf R, Yao Y, Spiess HW (2005) Nat Mater 4:635–641
5. Lippits DR, Rastogi S, Höhne GWH, Mezari B, Magusin PCMM (2007) Macromolecules 40:1004–1010
6. Martins JA, Zhang W, Brito AM (2006) Macromolecules 39:7626–7634
7. Chai CK, Auzoux Q, Randrianatoandro H, Navard P, Haudin J-M (2003) Polymer 44:773–782
8. Zhang W, Martins JA (2006) Macromol Rapid Commun 27:1067–1072
9. Martins JA, Zhang W, Brito AM (2010) Polymer 51:4185–4194
10. Bastiaansen CWM, Meyer HEH, Lemstra PJ (1990) Polymer 31:1435–1440
11. Liedauer S, Eder G, Janeschitz-Kriegl H, Jerschow P, Geymayer W (1993) Ingolic E Int Polym Process 8:236–244
12. Kumaraswamy G, Issaian AM, Kornfield JA (1999) Macromolecules 32:7537–7547
13. Somani RH, Yang L, Hsiao BS (2002) Physica A 304:145–157
14. Martins JA et al (2005) Rev Sci Instrum 76:105105
15. Krakowiak J (2009) Origin of melt memory effect and prediction of precursor structures dimensions in quiescent and sheared polyethylene melts: effect of crosslinking degree and catalyst type. Ph.D. thesis, Universidade do Minho, Braga
16. Wagner MH, Meissner J (1980) Makromol Chem 181:1533–1550
17. Brochard F, de Gennes PG (1992) Langmuir 8:3033–3037
18. Byelov D, Panine P, de Jeu WH (2007) Macromolecules 40:288–289
19. van Meerveld J (2004) Rheol Acta 43:615–623
20. Marrucci G (1996) J Non-Newt Fluid Mech 62:279–289
21. McLeisch TCB (2002) Adv Phys 51:1379–1527
22. de Gennes P (1984) Macromolecules 17:703–704
23. Ziabicki A, Alfonso GC (1994) Colloid Polym Sci 272:1027–1042
24. Häfele A, Heck B, Hippler T, Kawai T, Kohn P (2005) Strobl G Eur Phys J E 16:217–224
25. Eder G, Janeschitz-Kriegl H (1990) Liedauer S Prog Polym Sci 15:629–713
26. Janeschitz-Kriegl H, Ratajski E (1999) Wippel H Colloid Polym Sci 277:217–226
27. Martins JA (2010) Macromol Theory Simul 19:360–369
28. Martins JA (2011) J Macrom Sci Part B 50:769–794
29. Psarski M, Piorkowska E, Galeski A (2000) Macromolecules 33:916–932
30. Huo H, Meng YF, Li HF, Jiang SC, An LJ (2004) Eur Phys J E 15:167–175